Magnetic Investigations of Crystalline and Non Crystalline Iron Oxide Nanoparticles for Cancer Therapy

Saira Riaz[1)] and *Shahzad Naseem[2)]

[1), 2)] *Centre of Excellence in Solid State Physics, University of Punjab, Lahore, Pakistan*
[2)] saira.cssp@pu.edu.pk

ABSTRACT

Main difficulty in cancer therapy is the shortage of specificity of chemotherapeutic drugs for cancer cells. Large dose of drug with high efficiency are required to be inserted for achievement of efficient concentration in the tumor. Therefore, current efforts are focused on developing strategies for targeted drug delivery, including molecular and magnetic systems. In the recent development of nanobiotechnology, magnetic iron oxide nanoparticles have attracted increasing attention for use in biomedical applications. Nanoparticles are specifically beneficial for in vivo drug transport, due to their small size and large surface area. We here report sol-gel synthesis of iron oxide nanoparticles with variation in sol concentration as 0.2mM-1.0mM. XRD results confirm the formation of phase pure magnetite (Fe_3O_4) at sol concentration 0.2mM. Amorphous nanoparticles are observed at sol concentration 0.6mM while transition to crystalline maghemite nanoparticles is observed at sol concentration of 1.0mM. Amorphous nanoparticles show ferromagnetic behavior while transition to superparamagnetic behavior is observed for crystalline nanoparticles at sol concentrations 0.2mM and 1.0mM.

1. INTRODUCTION

During the last few years, magnetic nanoparticles have proven their applications in various biomedical applications including targeted drug delivery for cancer therapy, magnetic resonance imaging etc. (Ling et al. 2015, Li et al. 2015). Due to their reduced size magnetic nanoparticles with size less than 100nm exhibit unique properties in contrast to their bulk materials like large surface to volume ratio, high reactivity and surface energy (Hajba and Guttman 2016, Espinosa 2016, Fazio et al. 2016, Riaz et al. 2014a).

Magnetic nanoparticles have attracted much attraction of researchers as an efficient tool for cancer therapy. In comparison to conformist chemotherapeutic techniques, delivery system based on magnetic nanoparticles for cancer therapy exhibits less side effects. In addition, this system is capable of delivering therapeutic drugs to the required areas based on the ligands used (Hajba and Guttman 2016). For improving the drug delivery efficiency of magnetic nanoparticles there is a need to

synthesize magnetic nanoparticles with well-defined shape, size and composition along with stoichiometry (Riaz et al. 2014b, Fan et al. 2016, Hauser et al. 2015).

Among various magnetic nanoparticles, iron oxide (Fe_3O_4 and γ-Fe_2O_3) are widely used because of their biocompatibility and high saturation magnetization. Based on the size distribution, iron oxide nanoparticles are divided in three categories: 1) Superparamagnetic iron oxide nanoparticles 2) Ultrasmall superparamagnetic iron oxide nanoparticles 3) micrometer sized iron oxide particles. Both Fe_3O_4 and γ-Fe_2O_3 nanoparticles can be utilized for biomedical applications including cancer therapy (Hajba and Guttman 2016).

Both Fe_3O_4 and γ-Fe_2O_3 have cubic inverse spinel structure. In case of Fe_3O_4, Fe^{3+} cations are present on both octahedral sites and Fe^{2+} cations are present only on octahedral sites. Antiparallel arrangement of Fe^{3+} cations on octahedral and tetrahedral sites leads to cancellation of magnetic moment due to Fe^{3+} cations (Shete et al. 2015, Pati et al. 2015). The sole contributor to magnetization in Fe_3O_4 is Fe^{2+} cations. On the other hand, in case of γ-Fe_2O_3, only Fe^{3+} cations are present and in order to maintain charge neutrality vacancies are created on cationic sublattice. This results in reduced magnetization in γ-Fe_2O_3 as compared to Fe_3O_4 (Soares et al. 2015).

For utilizing iron oxide nanoparticles for cancer therapy it is extremely crucial to optimize the stoichiometry, shape and size of nanoparticles so that they can exhibit superparamagnetic behavior with high saturation magnetization (Riaz et al. 2014a,b). For this purpose we here report sol-gel synthesis of iron oxide nanoparticles prepared with variation in sol concentration as 0.2mM, 0.6mM and 1.0mM. Changes in magnetic and structural properties are correlated with variation in sol concentration.

2. EXPERIMENTAL DETAILS

Iron oxide nanoparticles were prepared using sol-gel method. Iron chloride was mixed in de-ionized water at ambient conditions. Ethanol was added to the above solution along with stirring at room temperature. The solution was heated at 50˚C to obtain iron oxide sol. Details of sol-gel synthesis were reported earlier (Riaz et al. 2013). Sol concentration was varied as 0.2mM, 0.6mM and 1.0mM. For nanoparticles synthesis, iron oxide sols were heat treated on hot plate at 80˚C to obtain iron oxide nanoparticles.

For phase analysis of iron oxide nanoparticles, Bruker D8 Advance X-ray diffractometer with Cukα (λ = 1.5406Å) was used. Magnetic analysis of iron oxide nanoparticles was carried out using Lakeshore's 7407 Vibrating sample magnetometer (VSM).

3. RESULTS AND DISCUSSION

Figure 1(a-c) shows XRD patterns for iron oxide nanoparticles prepared using sol concentrations 0.2mM, 0.6mM and 1.0mM. Peaks are indexed according to JCPDS card no. 72-2303 and 39-1346 for Fe_3O_4 and γ-Fe_2O_3 phases. Presence of diffraction peaks corresponding to planes (311), (400), (511) and (622) indicated the formation of phase pure Fe_3O_4 at sol concentration 0.2mM. As sol concentration was further increased to 0.6mM (Fig. 1(b)) the nanoparticles showed amorphous behavior and only

a small diffraction peak corresponding to (311) plane appeared. However, at this sol concentration shape of diffraction pattern is suggestive of the breakdown of existing phases and a restructuring process (Shah et al. 2014). This restructuring results in the formation of γ-Fe_2O_3 phase (Fig. 1(c)).

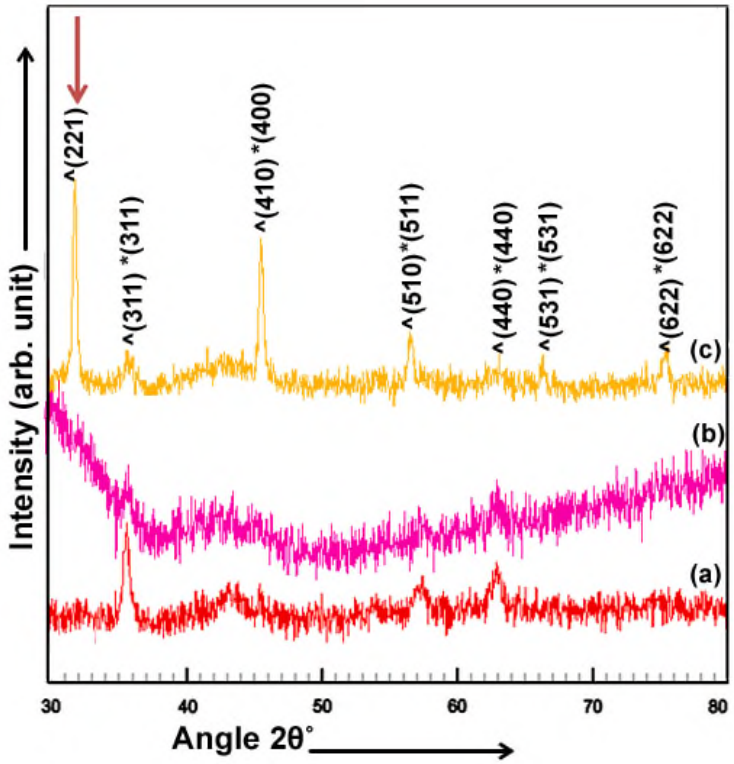

Fig. 1 XRD patterns for iron oxide nanoparticles prepared using sol concentration (a) 0.2mM (b) 0.6mM and (c) 1.0mM (*Fe3O4; ^ γ-Fe_2O_3)

Fe_3O_4 and γ-Fe_2O_3 phases have similar crystallographs the only difference is presence of vacancies at cationic sublattice in γ-Fe_2O_3 (Riaz et al. 2014a, Akbar et al. 2015). This makes it difficult to discriminate between the two phases on the basis of XRD patterns. However, careful analysis of JCPDS card nos. 72-2303 and 39-1346 indicate that there are certain diffraction angles present in γ-Fe_2O_3 that are not present in Fe_3O_4. In the sol-gel synthesized iron oxide nanoparticles with sol concentration 1.0mM (Fig. 1(c)) the presence of diffraction peak corresponding to plane (221) (marked by arrowhead in Fig. 1) indicated the formation of γ-Fe_2O_3 phase of iron oxide. This transition from Fe_3O_4 to γ-Fe_2O_3 occured by inward diffusion of oxygen anions and outward diffusion of iron cations. This forms a thin layer of γ-Fe_2O_3 on the surface of Fe_3O_4 nanoparticles (Riaz et al. 2014c, Tang et al. 2003). This process is observed as a restructuring process in Fig. 1(b). As this process proceeds with increase in sol concentration to 1.0mM phase transition to γ-Fe_2O_3 was observed (Fig. 1(c)).

Crystallite size (t) (Cullity 1956) and dislocation density (δ) (Kumar et al. 2011) were calculated using Eqs. 1-2

$$t = \frac{0.9\lambda}{B\cos\theta} \quad (1)$$

$$\delta = \frac{1}{t^2} \quad (2)$$

Crystallite size of 18.5nm was observed for nanoparticles prepared using sol concentration 0.2mM [Fig. 2]. Decrease in crystallite size to 11.12nm along with increase in dislocation density (Fig. 2(b)) was found as sol concentration increased to 0.6mM. This increased dislocation density is associated with restructuring process that was observed in Fig. 1(b). As restructuring process was completed with increase in sol concentration to 0.6mM increase in crystallite size to 21.3nm was observed. Nanoparticle synthesis in sol-gel process involves three basic steps that include nucleation, coalescence of nuclei to form particles and growth of particles. Increase in sol concentration leads to increase in number of colloidal particles. As the result of which probability of electrostatic interaction between the particles increases thus resulting in larger crystallites (Riaz et al. 2014c). But due to restructuring process that leads to phase transition from Fe_3O_4 to γ-Fe_2O_3 decrease in crystallite size was observed at sol concentration 0.6mM.

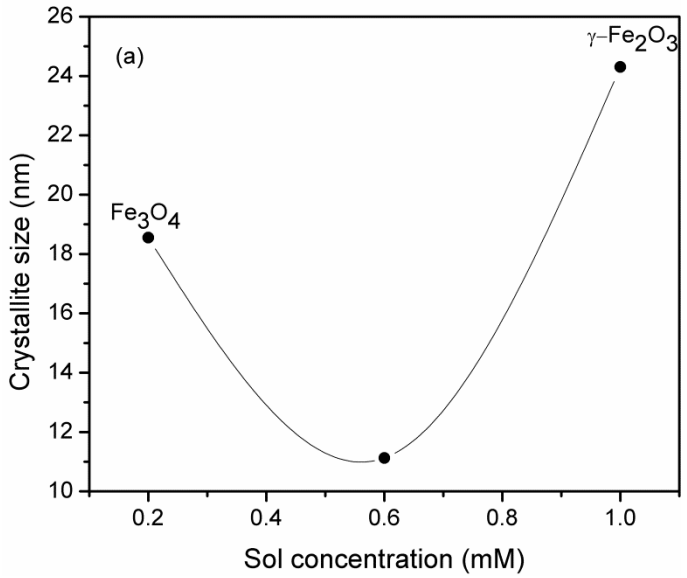

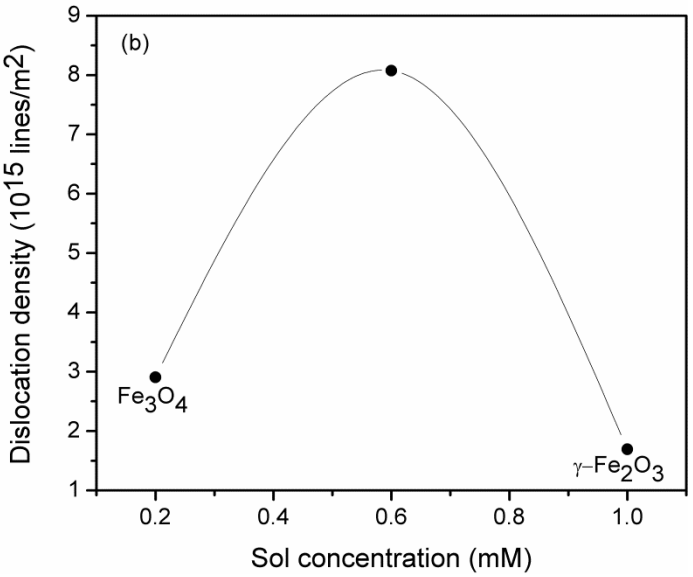

Fig. 2 (a) Crystallite size (b) dislocation density plotted at various sol concentration

Lattice parameters (*a*, *c*) and x-ray density (*ρ,* g/cm^3) (Cullity 1956) were determined using Eqs. 3-4

$$\sin^2\theta = \frac{\lambda^2}{4a^2}\left(h^2 + k^2 + l^2\right) \tag{3}$$

$$\rho = \frac{1.66042\Sigma A}{V} \tag{4}$$

Lattice parameter and unit cell volume are tabulated at various sol concentration in table 1. Lattice parameters are close to those reported for Fe_3O_4 and γ-Fe_2O_3 (JCPDS card no. 72-2303 and 39-1346). It can be seen in table 1 that lattice parameters decreases with increase in sol concentration. This decrease in lattice parameters arises due to different ionic radii of Fe^{3+} and Fe^{2+} cations. Ionic radius of Fe^{2+} cations is higher than that of Fe^{3+} cations (Criak 1975). This results in Fe^{3+}-O^{-2} spacing being less than that of Fe^{3+}-O^{-2} spacing and consequently decrease in lattice parameter along with transition from Fe_3O_4 to γ-Fe_2O_3 phase.

Table 1. Structural parameters for iron oxide nanoparticles

Sol concentration (mM)	Lattice parameter (Å)	Unit cell volume (Å^3)
0.2mM	8.38669	589.891
0.6mM	8.3645	585.221
1.0mm	8.355	583.229

Fig. 3 shows M-H curves for these iron oxide nanoparticles. Saturation magnetization and coercivity are plotted at various sol concentrations in Fig. 4. Nanoparticles prepared using sol concentration 0.2mM resulted in superparamagnetic behavior. If magnetic field is not applied, effective energy barrier for single domain particles is represented in Eq. 5 (Craik 1975).

$$E_a = K_{eff} V \tag{5}$$

Where, K_{eff} represents effective magnetic anisotropy constant and V is the volume of magnetic nanoparticles. E_a is the energy barrier that prevents the flipping of magnetic moment. When thermal activation energy of nanoparticles ($k_B T$) becomes equal to the effective energy barrier the nanoparticles exhibit superparamagnetic behavior (Craik 1975).

As sol concentration was increased to 0.6mM transition from superparamagnetic behavior to ferromagnetic behavior arose. This transition in magnetic properties arises due to restructuring process as was observed in Fig. 1(b). After restructuring process phase transition to γ-Fe_2O_3 nanoparticles leads to transition from ferromagnetic to superparamagnetic behavior with negligible coercivity (Fig. 3 and Fig. 4). It can be seen that nanoparticles prepared using sol concentration 0.2mM resulted in highest saturation magnetization. Decrease in magnetization at sol concentration is associated with phase transition from Fe_3O_4 to γ-Fe_2O_3 phase. In Fe_3O_4 both super exchange interaction and double exchange interactions coexists. Fe^{3+} cations on the octahedral and tetrahedral sites exhibits super exchange interactions and Fe^{3+} and Fe^{2+} cations exhibits double

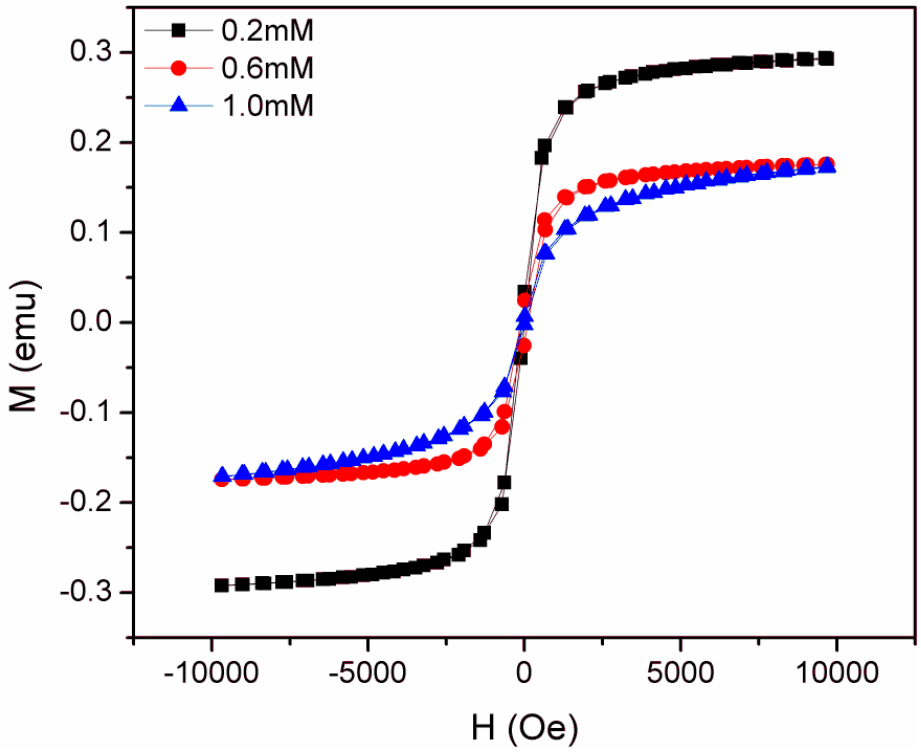

Fig. 3 M-H curves for iron oxide nanoparticles prepared using sol-gel method

exchange interactions. This results in cancellation of magnetization from Fe^{3+} cation. Fe^{2+} cations are sole contributors of magnetization in Fe_3O_4. With phase transition to γ-Fe_2O_3 phase vacancies are created thus resulting in decrease in magnetization. High magnetization and superparamagnetic behavior of these nanoparticles makes them a potential candidate for cancer therapeutic applications.

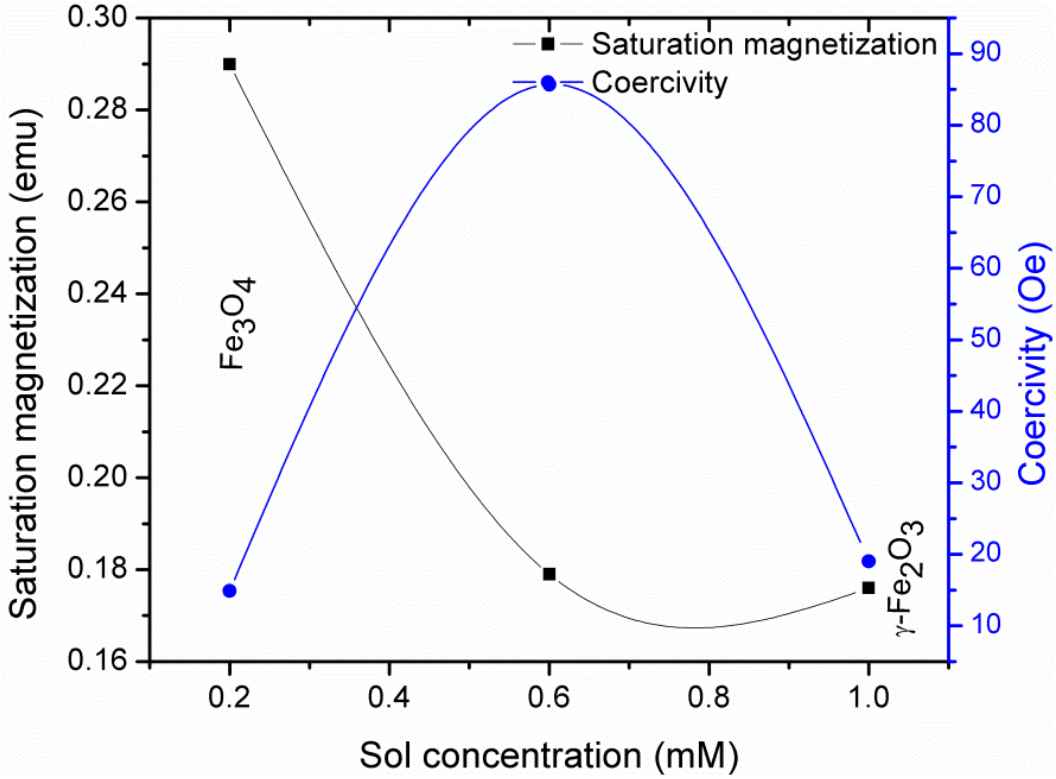

Fig. 4 Saturation magnetization and coercivity plotted as a function of sol concentration

4. CONCLUSIONS

Iron oxide nanoparticles were synthesized using sol-gel method with variation in sol concentration as 0.2mM, 0.6mM and 1.0mM. XRD results confirmed the presence of magnetite phase at sol concentration 0.2mM. As sol concentration increased, structural rearrangement occurred. This rearrangement of structure leads to phase transition to γ-Fe_2O_3 as sol concentration was increased to 1.0mM. Iron oxide nanoparticles prepared with sol concentrations 0.2mM and 1.0mM resulted in superparamagnetic behavior thus making these nanoparticles suitable for cancer therapy.

REFERENCES

Akbar, A., Riaz, S., Ashraf, R. and Naseem, S. (2015), “Magnetic and magnetization properties of iron oxide thin films by microwave assisted sol–gel route,” *J. Sol-Gel Sci. Technol.*, **74**,320–328.

Craik, D. J. (1975), “Magnetic Oxides,” New York: Wiley.

Cullity, B.D. (1956), “Elements of x-ray diffraction,” Addison Wesley Publishing Company, USA.

Espinosa, A.,Corato, R.D., Tabi, J.K., Flaud, P., Pellegrino, T. and Wilhelm, C. (2016), “Duality of Iron Oxide Nanoparticles in Cancer Therapy: Amplification of Heating Efficiency by Magnetic Hyperthermia and Photothermal Bimodal Treatment,” *ACS Nano*, **10**, 2436−2446.

Fan, H.L., Zhou, S.F., Qi, G.S. and Liu, Y.Z. (2016), “Continuous preparation of Fe_3O_4 nanoparticles using impinging stream-rotating packed bed reactor and magnetic property thereof,” *J. Alloy. Compd.*, **662**, 497-504.

Fazio, E., Santoro, M., Lentini, G., Franco, D., Guglielmino, S.P.P. and Neri, F. (2016), “Iron oxide nanoparticles prepared by laser ablation: Synthesis, structural properties and antimicrobial activity,” *Colloid Surf. A: Physicochem. Eng. Aspects*, **490**, 98–103.

Hajba, L. and Guttman, A. (2016), “The use of magnetic nanoparticles in cancer theranostics: Toward handheld diagnostic devices,” *Biotechnol. Adv.*, http://dx.doi.org/10.1016/j.biotechadv.2016.02.001

Hauser, A.K., Mathias, R., Anderson, K.W. and Hilt, J.Z. (2015), “The effects of synthesis method on the physical and chemical properties of dextran coated iron oxide nanoparticles,” *Mater. Chem. Phys.,* **160**, 177-186.

Kumar, N., Sharma, V., Parihar, U., Sachdeva, R., Padha, N. and Panchal, C.J. (2011) “Structure, optical and electrical characterization of tin selenide thin films deposited at room temperature using thermal evaporation method,” *J. Nano- Electron. Phys.*, **3**, 117-126

Li, S., Zhang, T., Tang, R., Qiu, H., Wang, C. and Zhou, Z. (2015), “Solvothermal synthesis and characterization of monodisperse superparamagnetic iron oxide nanoparticles,” *J. Magn. Magn. Mater.,* **379**, 226–231.

Ling, D., Lee, N. and Hyeon, T. (2015), “Chemical Synthesis and Assembly of Uniformly Sized Iron Oxide Nanoparticles for Medical Applications,” *Acc. Chem. Res.*, **48**, 1276−1285.

Pati, S.S., Singh, L.H., Ochoa, J.C.M., Guimaraesa, E.M., Sales, M.J.A., Coaquira, J.A,H., Oliveira, A.C. and Garg, V.K. (2015), “Facile approach to suppress γ-Fe_2O_3 to α-Fe_2O_3 phase transition beyond 600°C in Fe_3O_4 nanoparticles,” *Mater. Res. Express,* **2**, 045003.

Riaz, S., Akbar, A. and Naseem, S. (2013), “Structural, electrical and magnetic properties of iron oxide thin films,” *Adv. Sci. Lett.*, **19**, 828-833.

Riaz, S., Ashraf, R., Akbar, A. and Naseem, S. (2014a), “Microwave Assisted Iron Oxide Nanoparticles—Structural and Magnetic Properties,” *IEEE Trans. Magn.*, **50**, 2201504

Riaz, S., Akbar, A. and Naseem, S. (2014b), “Controlled Nanostructuring of Multiphase Core-Shell Iron Oxide Nanoparticles,” *IEEE Trans. Magn.*, **50**, 2300204

Riaz, S., Ashraf, R., Akbar, A. and Naseem, S. (2014c), “Free Growth of Iron Oxide Nanostructures by Sol-Gel Spin Coating Technique—Structural and Magnetic Properties,” *IEE Trans. Magn.*, **50**, 2301805.

Shah, S.M.H., Riaz, S., Akbar, A., Atiq, S. and Naseem, S. (2014), “Effect of Solvents on the Ferromagnetic Behavior of Undoped $BiFeO_3$ Prepared by Sol-Gel,” *IEEE Trans. Magn.*, **50**, 2200904

Shete, P.B., Patil, R.M., Tiwale, B.M. and Pawar, S.H. (2015), “Water dispersible oleic acid-coated Fe_3O_4 nanoparticles for biomedical applications,” *J. Magn. Magn. Mater.,* **377**, 406–410.

Soares, P.I.P., Lochte, F., Echeverria, C.E., Pereira, L.C.J., Coutinho, J.T., Ferreira, I.M.M., Novo, C.M.M. and Borges, J.P.M.R. (2015), “Thermal and magnetic properties of iron oxide colloids: influence of surfactants,” *Nanotechnology,* **26**, 425704.

Tang, J., Myers, M., Bosnick, K.A. and Brus, L.E. (2003), “Magnetite Fe_3O_4 Nanocrystals: Spectroscopic Observation of Aqueous Oxidation Kinetics,” *J. Phys. Chem. B*, **107***,* 7501-7506.